Available online at www.sciencedirect.com
SCIENCE DIRECT®
Journal of Organometallic Chemistry 691 (2006) 3362–3370
Journal of Organometallic Chemistry
www.elsevier.com/locate/jorganchem

Unusual conformational properties of 1,3-dimethyl-1,1,3,3-tetrakis(trimethylsilyl)trisilane: A preparative, X-ray, Raman spectroscopic and ab initio study

A. Dzambaski [a], J. Baumgartner [a], M. Flock [a], G. Tekautz [a], K. Hassler [a,*], W. Hassler [b]

[a] *Institute of Inorganic Chemistry, University of Technology, Stremayrgasse 16, A-8010 Graz, Austria*
[b] *Department of Mathematics, Karl Franzens University, Heinrichstrasse 36, A-8010 Graz, Austria*

Received 3 March 2006; received in revised form 19 April 2006; accepted 21 April 2006
Available online 29 April 2006

Abstract

The heptasilane $Me(SiMe_3)_2SiSiH_2SiMe(SiMe_3)_2$ was synthesized from $Me(SiMe_3)_2SiK$ and $H_2Si(OSO_2CF_3)_2$. Crystals suitable for a X-ray single crystal analysis could be grown, with the somewhat surprising result that the two dihedral angles $(H_3)CSiSi(H_2)Si$ are different in the crystal (24.58(10)° and 31.67(11)°). SiSiSi-bonds angles are widened, with values up to 117°. Ab initio calculations at the density functional B3LYP level employing 6-311G(d) basis sets predict minima for five conformers **1**–**5** with relative energies 0.0, 3.1, 8.2, 10.8 and 18.1 kJ/mol, respectively. Moreover, SiSiSiSi dihedral angles spanning the range 43.5–172.3° are predicted, reflecting the small forces which are required for distorting these angles.

In the Raman spectrum of a solution in toluene, three lines at 350, 340 and 330 cm^{-1} are observed in a wavenumber range which is typical for the SiSi-pulsation of methylated oligosilanes. The relative intensity ratio of the bands is temperature dependent, reflecting the changes in conformer concentrations that occur according to Boltzman's law. Supported by the ab initio calculations, the Raman band at 350 cm^{-1} is assigned to an 'averaged' conformer **1** and **2**, because a rapid interconversion between **1** and **2** has to be assumed due to a small barrier separating them. The bands with wavenumbers 340 and 330 cm^{-1} originate from conformers **3** and **4**. From the Raman spectra, relative energies 0.0 (**1** + **2**), 2.2 (**3**) and 6.3 (**4**) kJ/mol are deduced, the presence of **5** is not observed. Caused by solvent effects, these values differ somewhat from the ab initio results.

Keywords: Heptasilanes; Ab initio calculations; Raman spectroscopy; Rotational isomerism

1. Introduction

Understanding the conformational behaviour of longer flexible linear chains certainly is crucial for determining or predicting the behaviour of organic molecules. However, conformational properties are also important for chains composed of heavier backbone atoms such as silicon, germanium or tin. Research in the last 20 years focused primarily on oligo- and polysilanes which show interesting physical properties such as strong absorbance in the near UV which is commonly believed to be due to a σSiSi → σ*SiSi transition [1]. Semiempirical [2] and ab initio calculations [3] suggest that these σσ* excitation energies are strongly dependent on the backbone conformation of the chain. For example, the thermochromism of polysilane solutions has been attributed to the change of the relative population of all-*trans* segments with temperature. Usually, a bathochromic shift of the absorption in the near UV occurs upon cooling [4]. Further thermal studies of polysilanes revealed that polysilane conformational equilibria are rather complicated, providing evidence for a large number of phases, for instance for $[n\text{-octyl}_2Si]_n$ and $[n\text{-decyl}_2Si]_n$ [5].

The nature of the various phases of polysilanes was gradually revealed by the pioneering work of Michl and

* Corresponding author. Tel.: +43 316 873 8206.
E-mail addresses: karl.hassler@tugraz.at (K. Hassler), wolfgang.hassler@uni-graz.at (W. Hassler).

0022-328X/$ - see front matter © 2006 Elsevier B.V. All rights reserved.
doi:10.1016/j.jorganchem.2006.04.026

coworkers who studied tetrasilanes which are the simplest oligosilanes that offer backbone conformations. They reached the conclusion that in *n*-Si_4H_{10} [6] and *n*-Si_4Me_{10} [7] it is not the transition energy but the intensity of the transition to the four lowest excited states that is highly sensitive to the backbone conformation. Moreover, the ab initio calculations predicted the existence of three nonequivalent backbone conformers for the *n*-Si_4Me_{10} chain [7,8] with dihedral angles $\omega \sim 60°$ (*gauche*), $\omega \sim 90°$ (termed *ortho*) and $\omega \sim 165°$ (called *anti* at that time). Calculations also suggested the existence of a third (*ortho*) backbone conformer for the *n*-C_4F_{10} chain, for which the three nonequivalent conformers have been identified by direct observation of their mid-IR matrix-isolation spectra [9,10]. Similarly, three backbone conformers were predicted for $CF_3SiMe_2SiMe_2CF_3$ [11], $SnMe_3SiMe_2SiMe_2SnMe_3$ [12] and the chains $SiMe_3SiX_2SiX_2SiMe_3$ with X = H, F, Cl, Br and I [13]. In a Raman matrix-isolation study of $SiCl_3SiCl_2SiCl_2SiCl_3$ all three backbone conformers could be identified experimentally [14], and also in an electron diffraction study of *n*-Si_4Me_{10} [15].

A general analysis of linear *n*-A_4X_{10} chains predicted that for substituents X whose van der Waals radius is 0.8–1.0 times the AA bond length three rotamers will appear on the potential energy surface and that the splitting of the familiar gauche minimum into two is primarily due to 1,4-substituent van der Waals interactions [16]. The splitting of the *anti* minimum (backbone dihedral angle ω exactly 180°) into two around ±165° (called *transoid*) has been attributed to 1,3-steric interactions. Most recently, computational examination of *n*-Si_4Et_{10}, *n*-$Si_4Me_8Et_2$ and *n*-$Si_4Me_6Et_4$ suggested that for longer alkyl chain substituents there will be five backbone conformers with the backbone dihedral angles ω around 40°, 60°, 90°, 145° and 165° [17]. Consequently, the authors propose a new nomenclature for linear backbone conformations: *anti* ($\omega = 180°$), *transoid* ($\omega \sim 165°$), *deviant* ($\omega \sim 145°$), *ortho* ($\omega \sim 90°$), *gauche* ($\omega \sim 60°$), *cisoid* ($\omega \sim 40°$) and *syn* ($\omega = 0°$). A recent minireview summarizes these findings [18].

These results would seem to suggest that a Si_4 chain can adopt any pre-chosen dihedral angle ω as a local minimum on the potential energy surface provided that the substituents are selected in an appropriate way. A prerequisite probably is that not all 10 substituents should have the same size and electronegativity, though this might not be a strict condition. For instance, ab initio calculations for *n*-Si_4F_{10} predict a backbone conformer with $\omega \sim 120°$ (MP2/6-31G*), [16] a dihedral angle which is not predicted for any other *n*-tetrasilane with 10 identical substituents. It is of some note that a related conformer with $\omega \sim 115°$ is predicted for $SiMe_3SiF_2SiF_2SiMe_3$ [13].

To corroborate this hypothesis we have set out to prepare some oligosilanes with tetrasilane-substructures that possess at least three different types of substituents which in addition should be of vastly differing size and electronegativity and to examine their conformational properties by ab initio calculations, Raman spectroscopy and possibly X-ray diffraction. The substituents from which the tetrasilanes were composed comprise $SiMe_3$, Me, H, F, Cl, Br and I, and the substitution pattern is presented below.

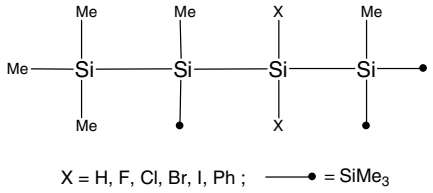

Moreover, all substituents either are monoatomic or possess a threefold rotation axis, excluding rotational isomers which differ by torsional angles of bonds within the substituents. Calculations on Si_4Et_{10} showed that substituent conformations also influence the torsion angles of the silicon backbone.

In this paper, we report on the title compound with X = H which was prepared from $H_2Si(OSO_2CF_3)_2$ and the silyl anion $(SiMe_3)_2MeSiK$ as shown below. We will report on the compounds with X = Ph, F, Cl, Br and I in a forthcoming publication.

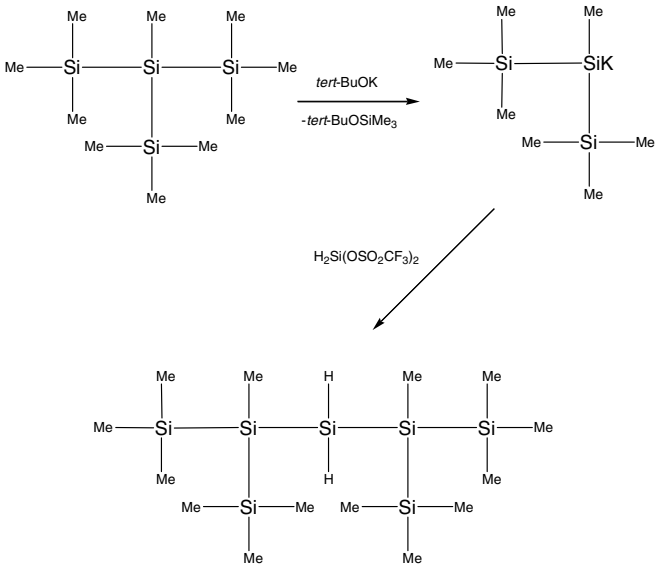

Raman vibrational spectroscopy was chosen as an experimental method for probing molecular conformations because of its short time scale of the order $\approx 10^{-13}$ s. For compounds containing bonds between third row elements, it is superior to NMR spectroscopy so powerful in organic chemistry. Most barriers hindering internal rotations of SiSi-bonds are so small that NMR spectroscopy, even at temperatures below −100 °C, simply is too slow for monitoring the process. For instance, the barrier for ring inversion of Si_6Me_{12} is so small that the splitting of the ^{13}C resonances due to axial and equatorial positions of the methyl groups can barely be observed at −165 °C [19]. A further difficulty is that at such low temperatures the solubilities of many silanes are too low for performing NMR spectroscopy.

2. X-ray diffraction

The molecular structure of the title compound is shown in Fig. 1, and selected molecular parameters are presented in Table 1. As expected, all SiSi bond lengths are in the normal range which is 232–236 pm. Some of the SiSiSi bond angles deviate strongly from the tetrahedral angle (109.5°), for instance the angle at the central atom Si(3) which is 116.9°. This is as large as the angles at the central Si-atom of $HSi[Si(SiMe_3)_2Me]_3$ which are 115.5°, 116.0° and 115.8°, respectively [20]. The angles within the two $Si(SiMe_3)_2Me$ groups (Si1Si2Si6 and Si5Si4Si7) are opened up also with values of 112.97° and 112.40° respectively, reflecting the strong van der Waal's interactions between the groups.

Molecular symmetries which are possible for $Me(SiMe_3)_2SiSiH_2SiMe(SiMe_3)_2Me$ are C_{2v}, C_2, or C_1. C_{2v} and C_2 demand identity of the two dihedral angles C4Si2Si3Si4 and C5Si4Si3Si2. This is not found in the crystal, as these two angles are −31.7° and −24.6° (see Table 1). They differ by about 7°. They are however reasonably close to the values of 44 and 26–28° predicted by the ab initio calculations for the two low energy conformers **1** and **2**, indicating a small barrier between them. One should keep in mind, however, that conformations in the solid state may not correspond to a local energy minimum of the undisturbed isolated molecule, especially if the related energy barriers of conformational changes are low and the space group of the crystalline phase is of low symmetry.

3. Ab initio calculations

Geometry optimizations were performed at the density functional B3LYP level with 6-311G(d) basis sets using GAUSSIAN03 [21]. Analytical frequency calculations ensured that the stationary points are actually minima on the potential energy surface (PES). A complete scan of the PES was performed at the restricted HF level using STO-3G basis sets keeping both Me–Si–Si–Si angles fixed in 20° steps.

The title compound can be looked upon as a substituted trisilane $(SiMe_3)_2MeSiSiH_2SiMe(SiMe_3)_2$ whose conformation can be characterized by two dihedral angles CSiSiSi. Its potential energy surface therefore may be compared with 1,3-disubstituted propanes and trisilanes. If the substituents X are halogen atoms, propanes as well as trisilanes show classical conformational minima with XCCC or XSiSiSi dihedral angles ω 1/ω2 of $\approx\pm60°$ and

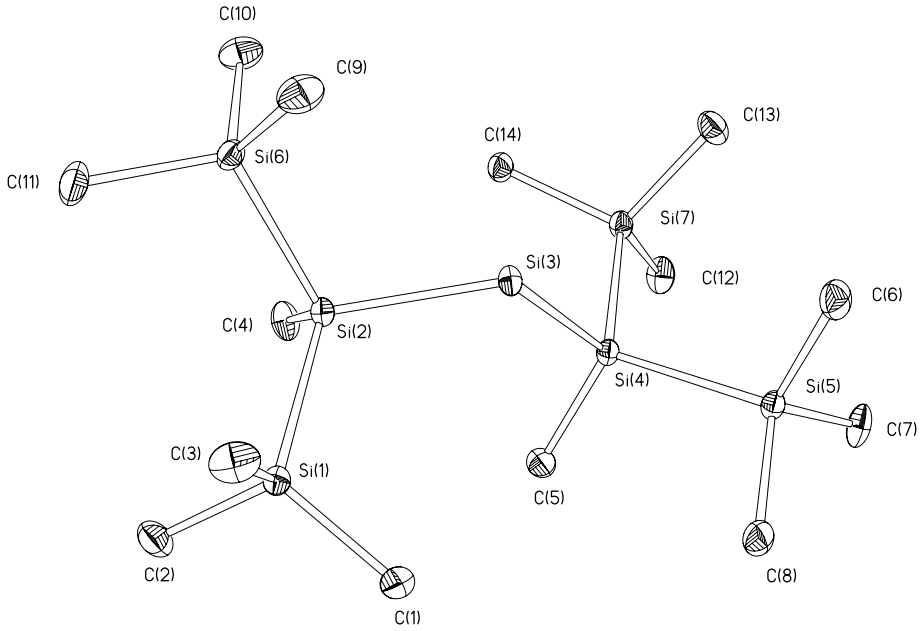

Fig. 1. ORTEP drawing of the molecular structure of $Me(SiMe_3)_2SiSiH_2Si(SiMe_3)_2Me$ with hydrogen atoms omitted for clarity.

Table 1
Important bond lenghts (pm), bond angles (°) and dihedral angles (°) for $Me(SiMe_3)_2SiSiH_2Si(SiMe_3)_2Me$

Bond length		Bond angle		Dihedral angle	
Si2Si3	234.11(12)	Si2Si3Si4	116.91(4)	C4Si2Si3Si4	−31.67(11)
Si3Si4	234.74(12)	Si6Si2Si3	106.41(4)	Si1Si2Si3Si4	89.90(5)
Si1Si2	234.69(10)	Si1Si2Si3	108.28(4)	Si6Si2Si3Si4	−148.49(4)
Si6Si2	234.19(13)	Si1Si2Si6	112.97(4)	C5Si4Si3Si2	−24.58(10)
Si5Si4	234.04(14)	Si5Si4Si3	106.28(5)	Si5Si4Si3Si2	−144.45(4)
Si7Si4	233.96(10)	Si7Si4Si3	105.45(4)	Si7Si4Si3Si2	96.04(5)
		Si5Si4Si7	112.40(4)		

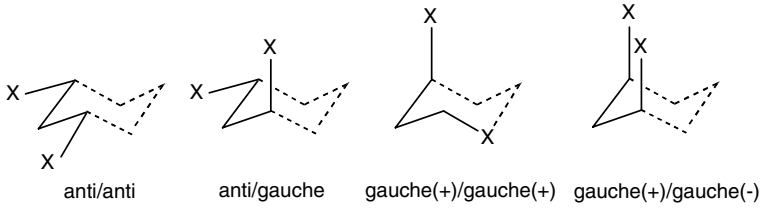

Fig. 2. Drawings of the conformers of 1,3-dihalopropanes and 1,3-dihalotrisilanes.

$\approx\pm180°$. Four spectroscopically different conformers, *anti*/*anti* ($\omega1 = \omega2 = 180°$), *anti*/*gauche* ($\omega1 = 180°$, $\omega2 = 60°$), *gauche*(+)/*gauche*(+) ($\omega1 = \omega2 = 60°$), and *gauche*(+)/*gauche*(−) ($\omega1 = 60°$, $\omega2 = -60°$), are expected to represent minima on the PES if optical isomerism is neglected. These are shown in Fig. 2 as parts of a cyclohexane ring for better visualization.

To gain some qualitative insight into the effects trimethylsilyl-substitution has on the two-dimensional potential energy surface of trisilanes, we performed calculations for $I_2HSiSiH_2SiHI_2$ and the title compound $(SiMe_3)_2MeSiSiH_2SiMe(SiMe_3)_2$. A 20° grid was used for the point-wise calculation of the PES for both compounds, allowing relaxation of all internal coordinates except the torsion angles HSiSiSi or (H_3)CSiSiSi which were fixed at pre-chosen values. A double Fourier series calculated by a least square method was then used to approximate the resulting surfaces and to represent them mathematically. Details are described in Section 5. Fig. 3 presents the result for $I_2HSiSiH_2SiHI_2$ (left) and the title compound $(SiMe_3)_2MeSiSiH_2SiMe(SiMe_3)_2$ (right). The difference between the two PES's is striking. Tetraiodotrisilane exhibits its classical behaviour with the four conformations *anti*/*anti*, *anti*/*gauche*, *gauche*(+)/*gauche*(+) and *gauche*(+)/*gauche*(−) representing the minima. Moreover, the surface appears very smooth. The PES of the title compound displays a much more rugged shape with a much larger number of minima, though many of them seem to be shallow.

So far, we were able to locate five minimum structures on the PES of the title compound, which are presented in Fig. 4 together with the relative energies and the CSiSiSi torsion angles $\omega1$ and $\omega2$. There surely are more, as the representation of the PES employing a Fourier series suggests. Stationary points can be found by calculating the partial derivatives, and geometry optimizations can then be carried out using the particular set of geometrical parameters as input. It turned out that many minima are very shallow and that we were unable to locate them on the level of theory we used. Due to restrictions of available disk space and computer time, MP2 calculations were out of range.

The calculated torsion angles for the two low-energy conformers (26°/26° and 28°/41°) agree quite well with the results of the X-ray experiments, which gave angles of 24.6° and 31.7° (Table 1). As the calculated values differ by mere 15°, the barrier separating the two conformers must be small and is easily overcome by the packing forces in the crystal.

In Fig. 5, the abundance of the calculated SiSiSiSi-torsion angles in the range $0° \leqslant |\omega| \leqslant 180°$ is illustrated with the help of a histogram. Numerical values for the angles are summarized in Table 2.

Maxima occur around 60° (*gauche*), 80–100° (*ortho*) and 140° (*deviant*) as predicted also for linear chains with alkyl substituents. However, additional minima on the PES exist, for instance, between 110–130 ° and 70–80°. The only range for which no torsion angles could be found is 0–40°. The histogram thus supports the hypothesis that by suitable choice of substituents minima for SiSiSiSi torsion angles spanning almost the whole range 0–180° can be introduced into an oligosilane. This is easily understood in terms of non-bonded interactions between the substituents. As the forces which are required to distort SiSiSiSi dihedral angles are very small, the combined energies of the substituent interactions determine the conformations of the Si-backbone.

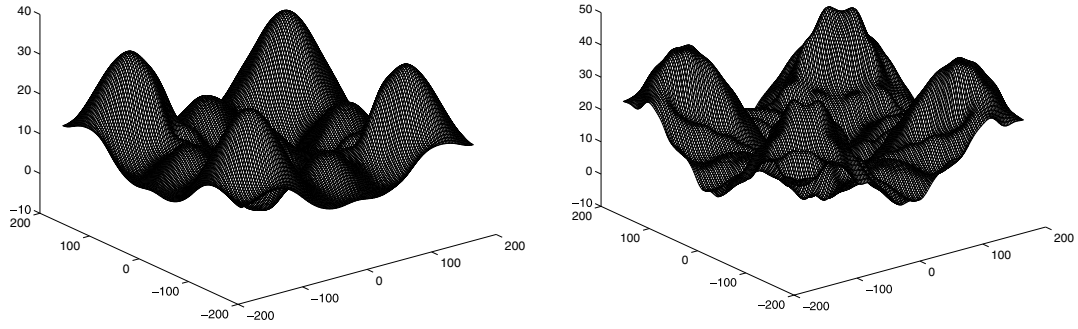

Fig. 3. PES of internal rotation of $I_2HSiSiH_2SiHI_2$ (left) and of the title compound (right). The energy is given in kJ mol^{-1}, torsion angles HSiSiSi and CSiSiSi vary between −180° and +180°.

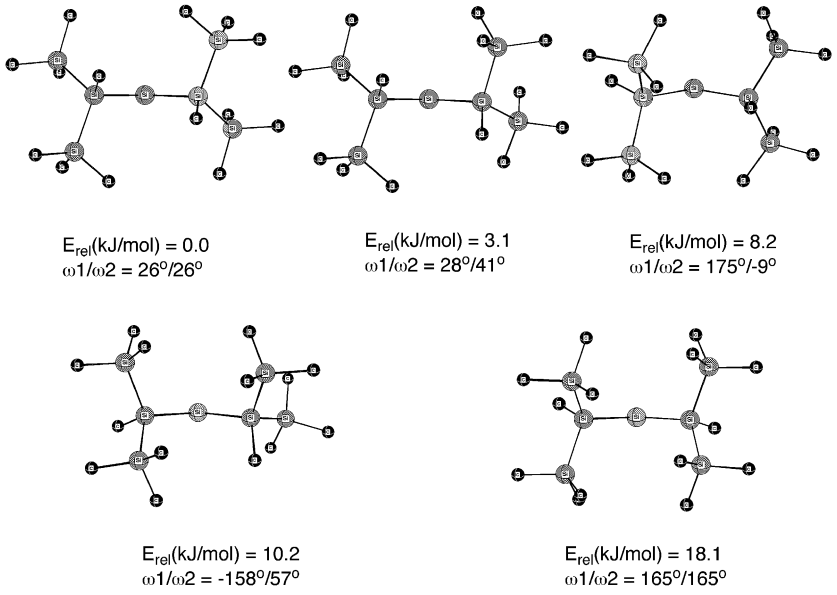

Fig. 4. Ball/stick models for the conformers **1**–**5** (numbered by increasing relative energies) of the title compound.

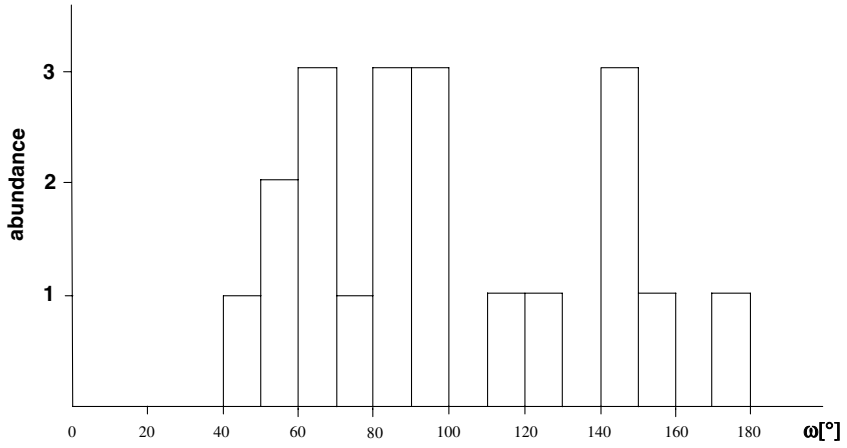

Fig. 5. Distribution of the calculated SiSiSiSi-torsion angles $|\omega|$ in the range $0° \leqslant |\omega| \leqslant 180°$ for the conformers **1**–**5** of the title compound.

Table 2
Predicted CSiSiSi and SiSiSiSi dihedral angles (°) for the conformers **1**–**5** of $Me(SiMe_3)_2SiSiH_2Si(SiMe_3)_2Me$

No.	C4Si2Si3Si4	C5Si4Si3Si2	Si1Si2Si3Si4	Si6Si2Si3Si4	Si5Si4Si3Si2	Si7Si4Si3Si2
1	26.3	26.3	144.5	−93.8	144.5	−93.8
2	27.6	41.3	145.6	−92.8	158.3	−79.0
3	175.0	−9.0	60.0	−69.9	111.4	−127.7
4	157.8	−56.9	43.5	−89.0	65.7	−172.3
5	164.7	164.7	50.6	−83.2	50.6	−83.2

4. Raman spectra and rotational isomerism

The Raman spectrum of the title compound in the wavenumber range 100–900 cm^{-1} is presented in Fig. 6. This range comprises the CSiSi and CSiC deformations $\leqslant$250 cm^{-1}, which do not allow to distinguish individual conformers. Due to their large number, massive band overlaps occur The same argument applies to the region 600–900 cm^{-1}, where SiC-stretching modes and methyl rocking modes are expected. The vibrations which are most sensitive to molecular conformations are the SiSi stretching modes which fall into the wavenumber range 300–500 cm^{-1}. In particular, it is the SiSi-stretch with the smallest wavenumber which possesses the highest Raman intensity that can be used for probing molecular conformations. It can be described as a 'symmetric' pulsation of the Si_7-skeleton in which all SiSi-bonds are involved, which is also the reason it possesses a high Raman intensity. For the title

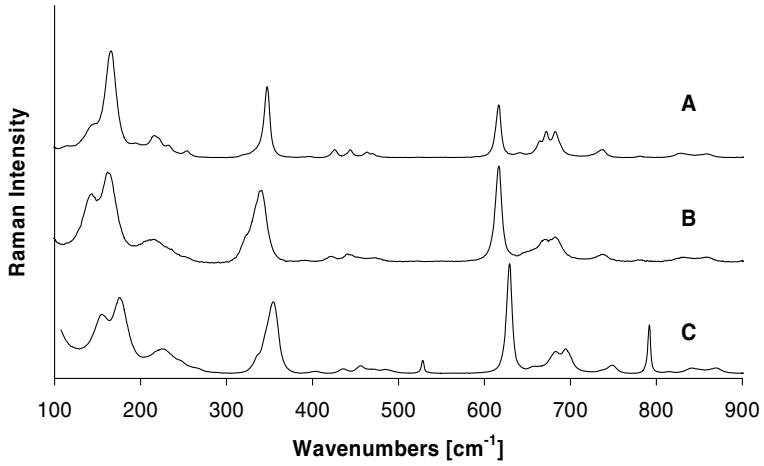

Fig. 6. Raman spectrum of the title compound in the range 100–900 cm^{-1}. (A) crystalline solid, RT; (B) melt at 100 °C; (C) solution in toluene, RT.

compound, this mode is located at roughly 330–350 cm^{-1}, depending on the conformations. The remaining SiSi-modes which appear in the range 400–500 cm^{-1} have only small intensities and are of little value for probing molecular conformations. ρSiH_2 vibrations, which appear in the wavenumber range 350–500 cm^{-1}, usually have very low Raman intensities and are also not suitable for investigating molecular conformations with Raman spectroscopy. Moreover, the ab initio calculations for the conformers **1**–**5** predict ρSiH_2-frequencies which are all in the narrow range 379–392 cm^{-1}. It is impossible to resolve them in the Raman spectrum.

In the crystalline solid (spectrum **A**), the 'symmetric' SiSi-pulsation appears as a sharp symmetric line located at 350 cm^{-1}, which of course means that a single conformer is present in the crystal. In the molten state (spectrum **B**), a shoulder at longer wavelength appears, whose intensity increases with temperature. In solution (spectrum **C**, in toluene) the overall shape of the band is similar. Upon closer inspection, it turns out to be split into three components with wavenumbers 350, 340 and 330 cm^{-1}, as illustrated in Fig. 7.

The relative intensities of the components in the band vary with temperature T, a sure sign that they originate from different conformers whose concentrations in the equilibrium mixture change with temperature according to Boltzmann's law.

The assignment of the observed Raman lines to SiSi stretching vibrations of individual conformers **1**–**5** relies on the results of the ab initio calculations. Table 3 summarizes the calculated wavenumbers and absolute Raman intensities for **1**–**5**. There are six SiSi-bonds in the molecule and consequently, six SiSi vibrations are calculated for each conformer.

Table 3 clearly demonstrates that for each conformer the SiSi vibration with the lowest wavenumber is predicted to possess the highest Raman intensitiy, which is corroborated by the Raman spectra (Fig. 6).

Moreover, the ab initio calculations predict that conformers **1** and **2** propably cannot be resolved with vibrational spectroscopy as the SiSi wavenumbers are too close. More importantly, the barrier separating them on the PES cannot be large because all the torsion angles of **1** and **2** differ by not more than 15° (Table 2). Therefore, a rapid interconversion of the two conformers is likely to occur, resulting in an averaged spectrum analoguous to averaging of NMR signals in the region of fast exchange. This follows from the theory of the activated complex (Eyring equation) which gives a pre-exponential factor $\chi T k_B h^{-1}$ of the order of 10^{10} depending on the value of χ (χ: transmission factor, T: temperature, k_B: Boltzmann constant, h: Planck constant). For a barrier of ≈2.5 kJ/mol (which is RT for 298 K), a lifetime of $\approx 10^{-11}$ s is expected. A supposed wavenumber difference of 10 cm^{-1} corresponds to a frequency difference $\Delta\nu = 3 \times 10^{11}$ Hz. On the time scale

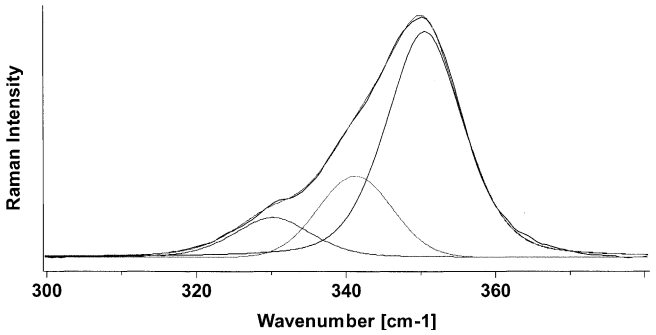

Fig. 7. Appearance and deconvolution of the 'symmetric' SiSi-pulsation mode of the title compound (solution in toluene, room temperature).

Table 3
Calculated wavenumbers (cm^{-1}) and Raman scattering activities ($Å^4$/AMU) in parentheses for the SiSi-stretching vibrations of conformers **1**–**5**

1	2	3	4	5
339(41)	336(27)	317(32)	313(30)	307(28)
341(0)	339(13)	350(4)	343(1)	337(0)
420(3)	418(3)	426(6)	*421(6)*	427(8)
435(10)	439(9)	432(8)	445(4)	441(4)
459(5)	453(7)	467(0)	456(5)	465(1)
468(4)	469(4)	476(7)	481(8)	485(3)

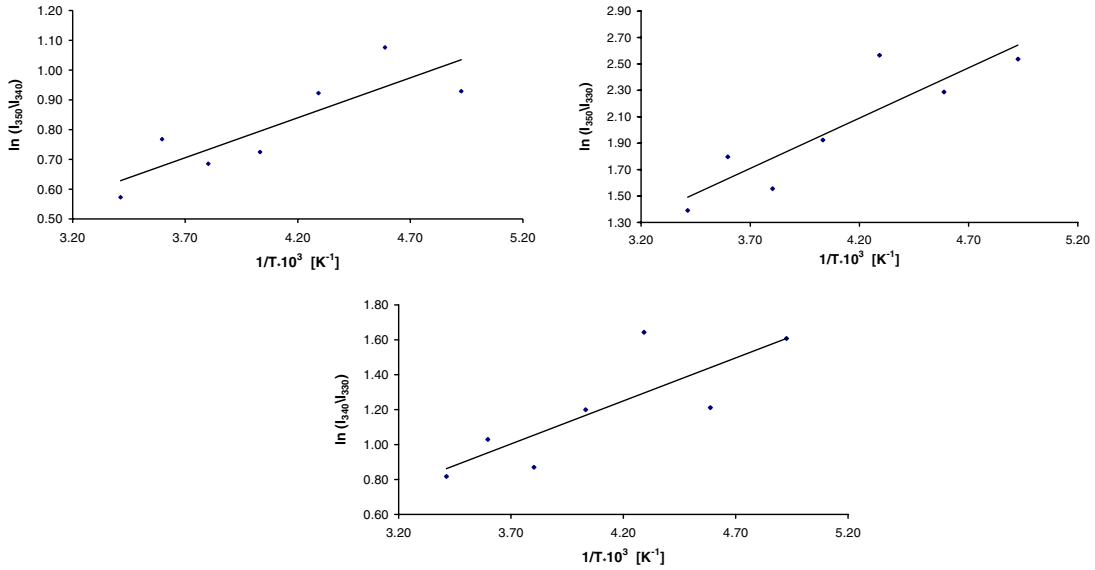

Fig. 8. Van't Hoff plots for the line pairs 350/340 cm^{-1} (left), 350/330 cm^{-1} (middle), and 340/330 cm^{-1} (right) for the temperature range 210–300 K.

of vibrational spectroscopy, the interconversion of the two conformers **1** and **2** thus is not a slow process.

If the barrier separating conformers is considerably larger than ≈2.5 kJ/mol, the interconversion is slow and each conformer will give its own vibrational spectrum. In this case, the enthalpy difference between conformers can be obtained from temperature dependent Raman spectra, because the intensity ratio of two bands belonging to different conformers varies with temperature according to the van't Hoff equation

$$\ln(I_a/I_b) = -\Delta H/RT + \text{const.}$$

Here, I_a and I_b are the intensities of bands belonging to conformer a and b, respectively. The van't Hoff equation in the form given above is derived under the assumption that $\Delta H(= H_a - H_b)$ and the Raman scattering coefficients for conformers a and b are independent of temperature.

Based on the ab initio calculations, the Raman lines at 340 and 330 cm^{-1} are assigned to rotamers **3** and **4**, respectively. The rotameric state **5** probably is not populated noticeably at ambient temperatures due to its high energy. Fig. 8 presents van't Hoff plots for the band pairs 350/340 cm^{-1} (left), 350/330 cm^{-1} (middle) and 340/330 cm^{-1} (right). Band areas obtained from deconvolutions using Lorentzian band shapes as shown in Fig. 7 were employed for the calculation of $\ln(I_a/I_b)$. The use of band heights gave essentially the same results. From the slopes of the least square fits, ΔH-values of -2.23 ± 0.62, -6.33 ± 1.47, and -4.10 ± 1.30 kJ/mol are obtained, which seem to be consistent as the difference between the first two gives the third one. They can be compared with the ab initio ΔE-values of ≈−7, ≈−9 and ≈−2.5 kJ/mol, respectively. Here, the energy of the averaged conformer **1** + **2** was assumed as ≈1.5 kJ/mol.

The agreement between experiment and ab initio calculations is not staggering, which may be attributed to several causes. First of all, the ab initio results refer to the gaseous state, whereas the Raman spectra come from the liquid state. Relative energies of conformers usually are solvent dependent, and is often observed that a more polar conformer is stabilized and a less polar conformer is destabilized in polar solvents, an effect which can even change the sign of ΔH. The calculated dipole moments of conformers **1**–**5** are 0.80, 0.93, 0.80, 1.16 and 1.0 Debye, respectively. They can differ by as much as 0.36 Debye, which means that solvent effects may not be negligible.

Second, the accuracy of the method depends on several premises. For instance, the bands attributed to the various conformers should be 'pure' bands which means that there is no overlap with bands from other conformers, be that fundamentals or overtones. If there is Fermi resonance between an overtone and a fundamental for a conformer, the intensity of the overtone is greatly enhanced and experimental ΔH-values will be influenced. As spectra for single conformers normally are not available, such effects cannot be accounted for. Moreover, the presence of an as yet unknown conformer might also obscure the spectra, an occurrence which we cannot rule out for the present heptasilane (see Section 3). As the statistical error limits which result from the least square fits of the data do not take into account these effects, the actual errors can be much larger.

It is of some note that in the molten state between 40 and 100 °C, the conformational behaviour of the title compound is quite different. This we attribute to the much stronger intermolecular forces, which of course are also responsible for the high viscosity of the melt. Besides a small wavenumber shift, the shape of the band located at ≈350 cm^{-1} is very similar to the band-shape in solution. Interestingly, it is the effects of temperature on relative intensities which are completely different. In the melt, three bands at 340, 332 and 323 cm^{-1} appear. With increasing temperature, the intensity ratio I_{340}/I_{332} increases, just

opposite to what is observed in solution. The experimental ΔH-value is +7.9 kJ/mol (solution: −2.2). The values for the pairs 340/323 and 332/323 are also different (−3.7 and −11.7 kJ/mol, respectively), but there is no change of sign. Evidently, the conformers (and their relative energies) present in the melt differ quite distinctly from the conformers found in solution. Unfortunately, these problems cannot be addressed with the help of ab initio calculations.

5. Experimental part

5.1. General remarks

All manipulations and reactions were carried out under anaerobic conditions using Schlenk techniques. Solvents were dried over Al_2O_3 using a column purification system of Innovative Technology.

^{1}H (299.95, 500.62 MHz), ^{13}C (75.43, 125.89 MHz) and ^{29}Si (59.59 MHz) NMR spectra were recorded on a VARIAN INOVA 300 and/or INOVA 500 spectrometer. Shifts are referenced against TMS (tetramethylsilane).

The mass spectrum was obtained with a HP 5971A coupled to a HP 5890 series II gas chromatograph.

Raman spectra were recorded with a JOBIN-YVON spectrometer equipped with a triple monochromator, a frequency doubled Nd:YAG laser (10 mW, 532 nm) and a CCD detector. Samples were distilled into 1 mm capillaries and then sealed under N_2. For recording the spectra at low and high temperatures the capillary was mounted on a copper block that could be cooled with liquid nitrogen and heated resistively. The temperature was monitored with a thermocouple. To avoid any deposition of ice, the copper block was placed inside an evacuable cryostat.

X-ray data were obtained with a BRUKER SMART Apex diffractometer. The structure was solved by direct methods (SHELTEX97) and refined by using full-martrix least-squares techniques based on F^2.

Elemental analyses were carried out with a VARIO EL by HERAEUS.

5.2. Synthesis

To a solution of 2.02 g (11 mmol) diphenylsilane in 25 mL of toluene 1.95 g (22 mmol) of trifluoromethanesulfonic acid CF_3SO_3H was added dropwise at 0 °C. The reaction mixture was then allowed to warm to room temperature and was stirred overnight to complete the reaction. The solution of bis(trifluoromethanesulfonyloxy)silane was then added to a toluene solution of 5.00 g (22 mmol) of methylbis(trimethylsilyl)potassium (prepared from $MeSi(SiMe_3)_3$ and tertBuOK [22]) at −78 °C over a period of one hour. The reaction mixture was then allowed to come to room temperature and was stirred for 48 h to complete the reaction. After filtration from the salts and removal of the solvent i.v., the bright yellow, oily residue was purified by fractionation in vacuo. The colorless oil solidified upon standing at room temperature, and the quality of the crystals was sufficient for a X-ray analysis. The yield was 2.00 g (44%).

B.p.: 110 °C/1 mmHg.

Elemental analysis $C_{14}H_{44}Si_7$ (409.11), calc./exp.: C, 41.10/41.25%; H, 10.84/10.88%.

^{29}Si NMR: $\delta(SiH_2) = -108.3$, $^1JSiH = 169$ Hz, $\delta(SiMe) = -85.4$, $\delta(SiMe_3) = -12.2$.

^{13}C NMR: $\delta(SiMe_3) = 0.1$; $\delta(SiMe) = -10.7$.

^{1}H NMR: $\delta(SiH_2) = 3.0$ (s, 2H), $\delta(SiMe) = 0.18$ (s, 6H), $\delta(SiMe_3) = 0.16$ (s, 36H).

MS (70 eV), *m/e* (%): 408 (1) [M^+−H], 334 (10) [M^+−$SiMe_3$−H], 319 (3) [M^+−$SiMe_3$−Me−H], 260 (100) [M^+−2$SiMe_3$−H], 245 (18) [M^+−$SiMe_3$−Me−H], 189 (12) [$Si(SiMe_3)Me^+$], 73 (69) [$SiMe_3^+$].

Crystal data: $C_{14}H_{44}Si_7$, triclinic, space group $P\,1$, $a = 9.808(2)$ Å, $b = 12.410(3)$ Å, $c = 12.454(3)$ Å, $\alpha = 86.28(3)°$, $\beta = 67.62(3)°$, $\gamma = 80.70(3)°$, $V = 1383.2\ (5)$ Å^3, $d_{calc.} = 0.982$ g/cm^3, $T = 100(2)$ K, final R indices [$I > 2\sigma(I)$]: $R_1 = 0.0429$, $wR_2 = 0.1080$, GOF = 1.164.

5.3. Two-dimensional discrete approximation of the PES by trigonometric functions

In this subsection, we briefly describe the approximation of the PES whose values are only known at a finite set of points. We assume that this set forms an equidistant quadratic lattice (ω_{1i}, ω_{2j}) with $1 \leqslant i,j \leqslant L$, and we denote by PES($\omega_{1i}$,$\omega_{2j}$) the value of the PES at the point (ω_{1i}, ω_{2j}). Since the PES is periodic in ω_1 and ω_2 we use trigonometric functions for approximation, and we impose the condition that the square mean becomes minimal (least squares approximation). The PES in the domain $-\pi \leqslant \omega_1 \leqslant \pi$, $-\pi \leqslant \omega_2 \leqslant \pi$ is thus approximated by a double Fourier series of the form

$$f = \sum_{\mu,\nu=1}^{2N+1} c_{\mu\nu} g_{\mu\nu},$$

subject to the condition

$$\sum_{i,j=1}^{L} [f(\omega_{1i}, \omega_{2j}) - \mathrm{PES}(\omega_{1i}, \omega_{2j})]^2 = \text{minimal}.$$

Here $g_{\mu\nu}(\omega_1, \omega_2) := \varphi_\mu(\omega_1)\varphi_\nu(\omega_2)$, where $\varphi_1(\omega) = 1$, $\varphi_{2j}(\omega) = \cos(j\omega)$ and $\varphi_{2j+1}(\omega) = \sin(j\omega)$ for all ω, $-\pi \leqslant \omega \leqslant \pi$. The real coefficients $c_{\mu\nu}$ then are determined by a system of $(2N+1)^2$ linear equations. By a detailed analysis it can be shown that this system of equations has a unique solution only if $L > 2N + 1$. It is plausible that such a condition must hold: In the extreme case when L is very small and N is large, we will find, in general, many different functions f approximating the PES exactly, i.e., functions f such that $f(\omega_{1i}, \omega_{2j}) = \mathrm{PES}(\omega_{1i}, \omega_{2j})$ for all i,j.

Our computations were performed on a personal computer using the MATLAB® software package. After having obtained the smooth proximum f, we determined its local

minima and maxima. In order to do this, we computed the partial derivatives $\partial f/\partial\omega_1$ and $\partial f/\partial\omega_2$, and depicted the function

$$g(\omega_1,\omega_2) = (\partial f(\omega_1,\omega_2)/\partial\omega_1)^2 + (\partial f(\omega_1,\omega_2)/\partial\omega_2)^2.$$

Note that the zeros of g correspond exactly to the points where $\partial f/\partial\omega_1$ and $\partial f/\partial\omega_2$ both vanish, that is, to the extremal points of f. From the graphical output we could then easily read off the local minima and local maxima of f, which were then used as starting points for geometry optimizations.

6. Supplementary data

The structure has been deposited with the Cambridge Crystallographic Center under the deposition number CCD 298667. Copies of this information may be obtained free of charge from The Director, CCDC, 12 Union Road, Cambridge CB2 1EZ, UK or e-mail: deposit@ccdc.cam.ac.uk or www: http://www.ccdc.cam.ac.uk.

Acknowledgement

Financial support of projects P 16112 (Karl Hassler) and P 16912 (Michaela Flock) by the Fonds zur Förderung der wissenschaftlichen Forschung (FWF), Vienna is gratefully acknowledged.

References

[1] R.D. Miller, J. Michl, Chem. Rev. 89 (1989) 1359.
[2] See for example H. Bock, W. Ensslin, F. Feher, R. Freund, J. Am. Chem. Soc. 98 (1976) 668;
K.A. Klingensmith, J.W. Downing, R.D. Miller, J. Michl, J. Am. Chem. Soc. 108 (1986) 7348.
[3] J.W. Mintmire, J.V. Ortiz, Macromolecules 21 (1988) 1189.
[4] See for instance L.H. Harrah, J.M. Zeigler, J. Polym. Sci. Polym. Lett. Ed. 23 (1985) 209;
P. Trefonas, J.R. Danewood Jr., R. West, R.D. Miller, Organometallics 4 (1985) 1318;
J. Michl, R. West, in: R.G. Jones, W. Ando, J. Chojnowski (Eds.), Silicon Containing Polymers, Kluwer Academic Publishers, Amsterdam, 2000, pp. 499–529.
[5] See for instance W. Chunwachirasiri, R. West, M.J. Winokur, Macromolecules 33 (2000) 9720.
[6] B. Albinsson, H. Teramae, H.S. Plitt, L.M. Goss, H. Schmidbaur, J. Michl, J. Phys. Chem. 100 (1996) 8681.
[7] B. Albinsson, H. Teramae, J.W. Downing, J. Michl, Chem. Eur. J. 2 (1996) 529.
[8] H. Teramae, J. Michl, Mol. Cryst. Liq. Cryst. 256 (1994) 149.
[9] B. Albinsson, J. Michl, J. Am. Chem. Soc. 117 (1995) 6378.
[10] B. Albinsson, J. Michl, J. Phys. Chem. 100 (1996) 3418.
[11] R. Zink, K. Hassler, A. Roth, R. Eujen, in: N. Auner, J. Weis (Eds.), Organosilicon Chemistry IV, Wiley–VCH, Weinheim, 2000.
[12] R. Hummeltenberg, K. Hassler, F. Uhlig, J. Organomet. Chem. 592 (1999) 198.
[13] R. Zink, G. Tekautz, A. Kleewein, K. Hassler, ChemPhysChem 6 (2001) 377.
[14] R. Zink, T.F. Magnera, J. Michl, J. Phys. Chem. 104 (2000) 3829.
[15] A.V. Belyakov, A. Haaland, D.J. Shorokhov, R. West, J. Organomet. Chem. 597 (2000) 87.
[16] F. Neumann, H. Teramae, J.W. Downing, J. Michl, J. Am. Chem. Soc. 120 (1998) 573.
[17] H.A. Fogarty, C.H. Ottoson, J. Michl, J. Mol. Struct. 556 (2000) 105.
[18] R. West, J. Organomet. Chem. 685 (2003) 6.
[19] D. Casarini, L. Lunazzi, A. Mazzanti, J. Org. Chem. 63 (1998) 9125.
[20] S. Chtchian, R. Kempe, C. Krempner, J. Organomet. Chem. 613 (2000) 208.
[21] M.J. Frisch, G.W. Trucks, H.B. Schlegel, G.E. Scuseria, M.A. Robb, J.R. Cheeseman, J.A. Montgomery Jr., T. Vreven, K.N. Kudin, J.C. Burant, J.M. Millam, S.S. Iyengar, J. Tomasi, V. Barone, B. Mennucci, M. Cossi, G. Scalmani, N. Rega, G.A. Petersson, H. Nakatsuji, M. Hada, M. Ehara, K. Toyota, R. Fukuda, J. Hasegawa, M. Ishida, T. Nakajima, Y. Honda, O. Kitao, H. Nakai, M. Klene, X. Li, J.E. Knox, H.P. Hratchian, J.B. Cross, C. Adamo, J. Jaramillo, R. Gomperts, R.E. Stratmann, O. Yazyev, A.J. Austin, R. Cammi, C. Pomelli, J.W. Ochterski, P.Y. Ayala, K. Morokuma, G.A. Voth, P. Salvador, J.J. Dannenberg, V.G. Zakrzewski, S. Dapprich, A.D. Daniels, M.C. Strain, O. Farkas, D.K. Malick, A.D. Rabuck, K. Raghavachari, J.B. Foresman, J.V. Ortiz, Q. Cui, A.G. Baboul, S. Clifford, J. Cioslowski, B.B. Stefanov, G. Liu, A. Liashenko, P. Piskorz, I. Komaromi, R.L. Martin, D.J. Fox, T. Keith, M.A. Al-Laham, C.Y. Peng, A. Nanayakkara, M. Challacombe, P.M.W. Gill, B. Johnson, W. Chen, M.W. Wong, C. Gonzalez, J.A. Pople, GAUSSIAN 03, Revision C.02, Gaussian, Inc., Wallingford, CT, 2004.
[22] C. Marschner, Eur. J. Inorg. Chem. 2 (1998) 221.